

n-Type Transition Metal Oxide as a Hole Extraction Layer in PbS Quantum Dot Solar Cells

Jianbo Gao,^{*,†,‡} Craig L. Perkins,[†] Joseph M. Luther,[†] Mark C. Hanna,[†] Hsiang-Yu Chen,[†] Octavi E. Semonin,^{†,§} Arthur J. Nozik,^{†,§} Randy J. Ellingson,[‡] and Matthew C. Beard^{*,†}

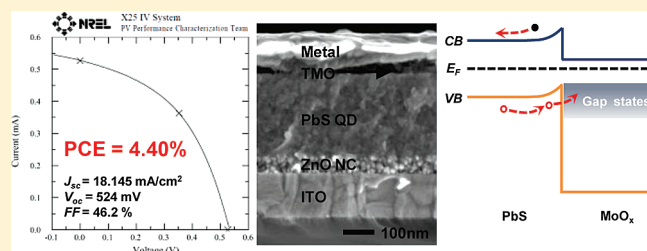
[†]National Renewable Energy Laboratory, Golden, Colorado, United States

[‡]Department of Physics and Astronomy, Wright Center for Photovoltaics Innovation and Commercialization, University of Toledo, Toledo, Ohio, United States

[§]Chemistry Department, University of Colorado, Boulder, Colorado, United States

ABSTRACT: The n-type transition metal oxides (TMO) consisting of molybdenum oxide (MoO_x) and vanadium oxide (V_2O_x) are used as an efficient hole extraction layer (HEL) in heterojunction ZnO/PbS quantum dot solar cells (QDSC). A 4.4% NREL-certified device based on the MoO_x HEL is reported with Al as the back contact material, representing a more than 65% efficiency improvement compared with the case of Au contacting the PbS quantum dot (QD) layer directly. We find the acting mechanism of the hole extraction layer to be a dipole formed at the MoO_x and PbS interface enhancing band bending to allow efficient hole extraction from the valence band of the PbS layer by MoO_x . The carrier transport to the metal anode is likely enhanced through shallow gap states in the MoO_x layer.

KEYWORDS: Transition metal oxide, hole extraction layer, quantum dot, solar cell, band bending, gap states



Recently we reported the existence of two opposing diodes in heterojunction ZnO/PbS quantum dot solar cells (QDSCs): a desirable forward diode at the heterojunction formed between a ZnO nanocrystal (NC) layer and the PbS QD layer, while a Schottky barrier forms between the PbS QD layer and the anode in the opposite direction.^{1,2} Holes accumulate at the PbS/anode interface due to the Schottky barrier Φ_b , as shown in Figure 1a. The Schottky-barrier height depends on QD size, such that the hole extraction barrier increases as the QD diameter decreases. Thus the undesired barrier can be reduced by using larger QD sizes (smaller band gap). However, the device power conversion efficiency (PCE) then suffers from a reduced open circuit voltage (V_{oc}). Therefore, we have investigated avenues toward a hole extraction layer that blocks electrons and works well with any QD bandgap. A traditional approach to introduce a HEL between an active layer and anode is to select a material with a HOMO and LUMO that are closer to the vacuum level than those of the active layer.³ For example, Choi, et al.⁴ and Leschkes et al.⁵ reported PbSe QD solar cells, where PEDOT/PSS or α -NPD layers were used to block electrons and transport holes based on their shallow HOMO and LUMO levels, respectively. In this report, we adopt a different approach based on a transition metal oxide HEL used previously in organic LEDs^{6–9} and organic solar cells. We demonstrate that a layer of substoichiometric MoO_3 ^{10–13} or V_2O_5 ^{14–16} becomes n-type and can be used to efficiently enhance hole extraction in heterojunction ZnO NC/PbS QDSCs by injecting an electron from the HEL into the valence band of the PbS QD layer, thus effectively extracting the positively charged hole. In contrast to a device employing an Au anode and no HEL (PCE = 2.66%, J_{sc} = 15.5 mA/cm²), the use of the MoO_3 or V_2O_5 HEL significantly

improves the PCE by more than 65% to PCE \sim 4.4% with J_{sc} of 18 mA/cm². Furthermore, we show that the device PCE is independent of anode for Au, Ag, and Al, which offers the opportunity to replace the high work function common precious metal Au anode contact with TMO/Al while maintaining device performance.

J–V Characteristics under Light Illumination. Details of the QD synthesis are described in the nanocrystal synthesis section. Nanocrystalline ZnO was spin-coated on patterned ITO glass slides (Thin Film Devices, Anaheim, CA) and then heated on a hot plate in air to 260 °C for 30 min. The PbS QD layer (3.5 nm diameter QDs) was deposited as described before^{1,2} with slight modification. The precise PbS QD layer formation will be described in a future publication however,¹⁷ the results of the TMO work reported here are independent of the modified PbS QD formation and the results will be the same for the EDT layer-by-layer formation that we have previously reported.^{1,2} The PbS film was then loaded from ambient air into the evaporation chamber. The TMO film was thermally evaporated at a rate of 0.5 Å/s at a base pressure of $\sim 10^{-6}$ Torr. The final thickness, unless otherwise noted, was 10 ± 1 nm. The evaporation sources were acquired from Aldrich (99.99% molybdenum oxide and 99.99% vanadium oxide powder). In the following, instead of MoO_3 and V_2O_5 , we will use the notation of MoO_x and V_2O_x to represent the stoichiometry of thermally evaporated TMO films. Nonstoichiometric TMO films are usually obtained from thermal evaporation due to the oxygen deficient environment.¹⁸ The

Received: May 10, 2011

Revised: June 11, 2011

Published: June 20, 2011

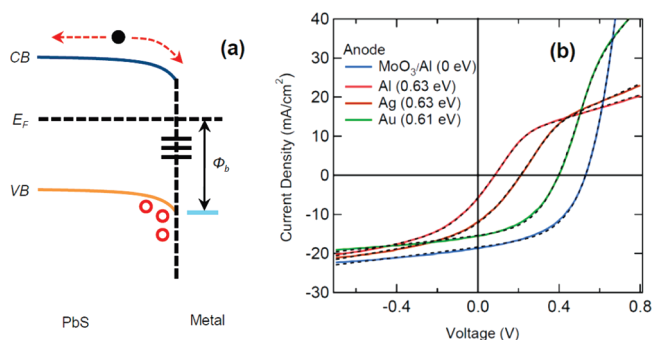


Figure 1. (a) Schematic energy diagram of the unintentional Schottky diode at the PbS/metal interface. (b) Measured light J - V characteristics under 100 mW/cm^2 white light illumination for devices with various anodes (solid lines). The dotted lines are fitting curves based on a two-diode model published in our previous report.¹ The values in parentheses are the fitting results of Schottky junction hole injection barrier height.

Table 1. PbS QD Solar Cell Operation Parameters for Devices with Various Anodes

anode	V_{oc} (mV)	J_{sc} (mA/cm ²)	FF (%)	PCE (%)
10 nm MoO _x /Al	524.5	17.9	48.7	4.46
20 nm MoO _x /Al	549.5	17.9	41.5	4.20
10 nm MoO _x /Ag	530.4	18.7	47.6	4.53
10 nm MoO _x /Au	540.0	17.4	47.0	4.41
10 nm V ₂ O _x /Al	525.9	19.1	44.8	4.48
Al	83.8	5.6	26.0	0.12
Ag	212.1	11.4	30.2	0.73
Au	399.5	15.5	43	2.66

amount of oxygen in our films is difficult to determine due to the abundance of background oxygen, however Cheung et al.¹⁸ has determined similarly deposited MoO_x to have a stoichiometry of MoO_{2.6}. Top contacts were thermally evaporated with or without a TMO layer at a base pressure of 10^{-7} Torr. The blue curve of Figure 1b shows the J - V characteristics for a device structure of ITO/ZnO NC/PbS QD/MoO_x/Al with MoO_x as the HEL layer under 100 mW/cm^2 white light illumination. For comparison, we also show device J - V characteristics without MoO_x using Al, Ag, and Au as anodes. The light J - V characteristics of devices using MoO_x/Au and MoO_x/Ag anodes have similar shapes as the curve for the MoO_x/Al anode in Figure 1b (not shown in the plot). The dotted lines are a best fit of a two-diode model to our data and the values in parentheses are the calculated Schottky-junction hole injection barrier height. (see ref 1 for details)

Figure 1b clearly shows the effect of the HEL. The J - V characteristics for the Al, Ag, or Au contact show a roll-over effect above the V_{oc} due to the Schottky induced hole-transport barrier (Φ_b), see Figure 1a, at the metal contact that is removed with the addition of the TMO layer between the PbS and anode. Without the TMO layer, holes accumulate at the PbS QD/anode interface while electrons can be collected in both directions (by anode or cathode), causing increased recombination at the anode. By inserting MoO_x the roll-over is eliminated, corresponding to higher fill factor (FF), V_{oc} , and short circuit current (J_{sc}). All device parameters are listed in Table 1, indicating that without the HEL the device performance depends heavily on the anode material.

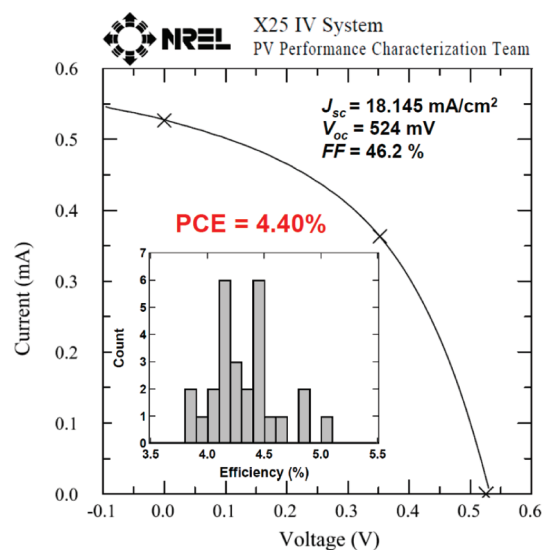


Figure 2. Measured I - V (raw current, rather than current density as used throughout the rest of this manuscript) characteristics of 4.4% certified device by NREL. A copper aperture of area 2.9 mm^2 was placed over the 11 mm^2 area device to accurately define the illumination area that prevents photocurrent generated outside the active area of the cell from contributing. Device operation parameters are listed in the top corner. The bottom inset is a histogram of 27 devices including the PCE of 5.04% lab champion device.

With Al as the anode, the device only yields 0.12% PCE. Higher work function anodes such as Ag or Au can be used to minimize the back-junction effect, but the PCE remains relatively low (2.66% for Au and 0.73% for Ag). By inserting 10 nm MoO_x layer and with Al as contact, the V_{oc} , FF, and J_{sc} significantly improve to 524.5 mV, 48.7%, and 17.9 mA/cm^2 , respectively. In contrast, similar J - V characteristics are observed for Au or Ag devices with MoO_x layer. As a result, the PCE of these devices, independent of top contact material, increased to $\sim 4.4\%$. In Figure 2, we show the I - V characteristics of a device, certified by NREL and measured under ambient air conditions. To the best of our knowledge, this device with $\sim 4.40\%$ PCE is the highest-efficiency certified QD solar cell to date. Our lab champion device PCE is 5.04%, and a histogram (based on 27 similar devices with various metal anodes but all containing the HEL) is shown in the inset.

To further characterize the MoO_x HEL effect, we used a two-diode model to simulate the measurement J - V characteristics of Figure 1b (solid lines), where the dotted lines are fitting curves. The significance of the fitting results is the hole barrier height reduction from more than 0.60 eV for all contacts to 0 eV by inserting MoO_x as the HEL, (barrier heights are shown in parentheses in Figure 1b), indicating that inserting MoO_x completely removes the back diode. Inserting the MoO_x layer into the device stack introduces two new interfaces: one between the PbS QD layer and the MoO_x layer, and another between the MoO_x and the anode contact layer. However, as shown in Table 1, the resulting device PCE is independent of top contact materials, which is in agreement with other results where WoO_x¹² or MoO_x¹³ were used as HELs in bulk heterojunction PCBM/P3HT solar cells. Therefore, we conclude that the hole extraction mechanism depends only on the PbS/MoO_x interface, not the MoO_x/metal anode interface.

UPS Measurement and HEL Mechanisms. To understand the nature of MoO_x as an efficient HEL, we used ultraviolet

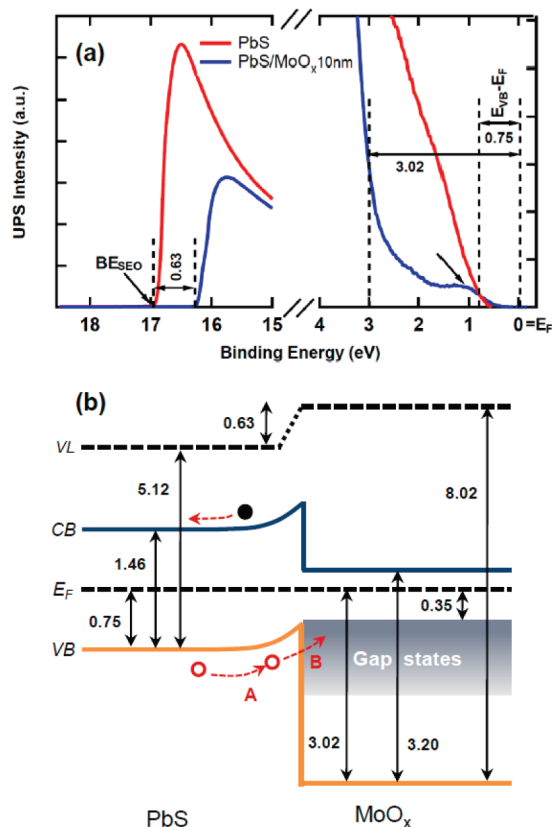


Figure 3. (a) UPS cutoff spectra of PbS and PbS/MoO_x. Left panel is the work function and right panel is the valence band region, respectively. The work function is calculated by subtracting the secondary emission binding energy offset (BE_{SE0}) from excitation beam (21.2 eV) and the energy difference between VB to Fermi level is calculated by the linear portion of the low binding energy side of the proper VB peak relative to the energy axis. (b) Schematic energy diagram of interfacial layers PbS/MoO_x deduced by the UPS data in panel (a). PbS QD and MoO_x band gap are 1.46 eV from PbS thin film optical absorption spectrum and 3.2 eV from literature,¹⁹ respectively. Two mechanisms may contribute to the hole extraction: A, the dipole enhanced band-bending to assist hole extraction at the PbS interface; B, gap states due to oxygen vacancy in MoO_x as hole transport levels.

photoemission spectroscopy (UPS) to determine the interfacial energy levels between MoO_x and PbS QD layer. Figure 3a shows representative UPS data of a PbS film and PbS with 10 nm MoO_x.

The PbS layer work function (ϕ) is determined by intersection of the secondary electron cutoff occurring at high binding energy. The VB energy with respect to E_F is found extrapolated by the linear portion of the low binding energy side of the proper VB peak to the energy axis,²⁰ indicated in Figure 3a. The measured PbS ϕ is 4.37 ± 0.03 eV. Upon depositing 10 nm of MoO_x, the secondary electron cutoff shows that ϕ increases by 0.63 to 5.0 eV. This vacuum level shift is attributed to the formation of an interfacial dipole between PbS and MoO_x layers resulting from a charge transfer interaction similar to the MoO_x/organic case.^{19,21–24} The energy difference between the VB and Fermi level (E_F) for MoO_x is 3.02 eV as shown in Figure 3a, indicating that MoO_x is an n-type material since $CB - E_F$ is only 0.18 eV, which is in agreement with other reports.^{21,22} The measured MoO_x ϕ value of 5.0 eV is lower than Kahn and So's result of 6.86 and 6.75 eV, respectively.^{21,23} The discrepancy may result from oxygen, water, and other molecules adsorbed on our MoO_x

layers, in our case, the MoO_x layers are deposited under rough vacuum at 10^{-6} Torr and are briefly exposed to air before anode deposition. A recent study by So et al. shows that the ϕ of clean MoO_x decreases more than 1 eV with air or oxygen exposure.²⁴ Therefore, we find that the MoO_x layer is a heavily doped n-type material with a deep ϕ of 5.0 eV. The deduced schematic energy diagram for PbS QD/MoO_x interface is shown in Figure 3b.

As shown in Figure 3b, the VB of the MoO_x layer is far below the VB of the PbS layer since MoO_x is a wide band gap with $E_g = 3.2$ eV.¹⁹ Such a wide band gap would be expected to result in a large hole injection barrier at the PbS/MoO_x interface, which should reduce the device performance instead of increasing the PCE. A possible reason for the significant PCE increase with the insertion of the MoO_x layer is due to the interfacial dipole, which enhances band bending at the interface between MoO_x and PbS QD layer, as shown in Figure 3b, allowing more efficient hole collection at the PbS/MoO_x interface. A similar mechanism was also proposed in MoO_x/organic interface.^{11,23} Furthermore, as shown in Figure 3a right panel, there is a peak around 1.1 eV with edge of 0.35 eV due to gap states, which was also reported from UPS studies conducted by Kanai¹⁹ and Irfan²⁴ et al. These gap states are oxygen vacancies that donate electrons to the conduction band since the molybdenum atoms neighboring oxygen vacancies are accepting some amount of electrons.¹⁹ The gap states nearly align with the VB of the PbS layer at the PbS/MoO_x interface. The combination of the interfacial dipole plus the gap states provides hole-transporting levels from the PbS layer to the top anode contact through the MoO_x layer simply by injecting electrons into the PbS VB hole sites.^{19,25} To reinforce the notion of electron transport in the MoO_x channel, we show with a thicker MoO_x layer of 20 nm, there is no apparent decrease in device performance (see Table 1) implying an unlikelihood of a tunneling process through the MoO_x. Furthermore, for the sake of generality we demonstrate that another TMO of V₂O₅, an n-type material with high ϕ , also works in the same way in this system. As listed in Table 1, the device operation parameters have similar value as the MoO_x HEL with 10 nm V₂O₅ and Al as top contact.

In conclusion, we report that an n-type transition metal oxide MoO_x or V₂O₅ layer can be used to enhance hole extraction efficiency in heterojunction ZnO NC/PbS QD solar cells. An NREL-certified record device with 4.4% PCE is achieved and reported here. The interface between PbS/MoO_x characterized by UPS indicates that an n-type MoO_x layer with 5 eV work function may form band bending with the PbS layer due to a large interfacial dipole. We characterize shallow gap states in MoO_x which may contribute to the efficient hole extraction.

Nanocrystal Synthesis. Synthesis of ZnO NCs was carried out by adding 4.4 g of ZnAc to 200 mL of MeOH, heating to 60 °C and dropwise adding 100 mL of a 0.4 M KOH solution in MeOH. The solution was stirred at 60 °C for 2 h. The particles were extracted via centrifuge and resuspended in MeOH. This was repeated three times, and finally the dry ZnO powder was dispersed in 40 mL of CHCl₃.

We synthesized PbS QDs with a first exciton peak at 850 nm (1.46 eV) by adding 0.47 g of PbO, 2 g of oleic acid, and 10 g of octadecene (ODE) to a three-neck round-bottom flask. This mixture was heated to 120 °C under vacuum for 2 h and then kept under N₂. In a glovebox, 180 μ L of hexamethyldisilathiane was mixed with 5 mL of ODE and loaded into a syringe. The contents of the syringe were injected into the flask and immediately the heating mantle was removed while the QDs were

cooled to room temperature. The reaction solution was mixed with 10 mL of hexane and 20 mL of ethanol and centrifuged to extract the QDs. Hexane and ethanol were used again for an additional purification step, and the QDs were then suspended in hexane with oleate molecules capping the QDs and stored in air or a N₂ desiccator until use.

UPS Measurements. Optimized device thickness PbS films are prepared by layer-by-layer fashion as described in device fabrication section on glass substrates with 100 nm of Au. For PbS QD/MoO_x films, MoO_x was evaporated onto the top of the PbS QD film at a rate of 0.02 nm/sec with a base pressure of 1×10^{-6} Torr and exposed to air. UPS data were obtained on a modified Physical Electronics 5600 photoemission system that has been incorporated into a custom-built ultrahigh vacuum (UHV) with a base pressure of 10^{-10} Torr. A SPECS UVS 10/35 He lamp at 21.2 eV was used as UPS source.

AUTHOR INFORMATION

Corresponding Authors

*Matt.Beard@nrel.gov; jianbo.gao@nrel.gov.

ACKNOWLEDGMENT

The authors thank B. Gregg for technical support on transition metal oxide deposition. J.G., H.Y.C., and R.J.E. were supported by a PV seed fund provided by the NCPV program at NREL. J.M.L., A.J.N., and M.C.B. were supported by the Center for Advanced Solar Photophysics an Energy Frontier Research Center funded by U.S. DOE Office of Science. DOE funding was providing to NREL through contract DE-AC36-08GO28308.

REFERENCES

- (1) Gao, J.; Luther, J. M.; Semonin, O. E.; Ellington, R. J.; Nozik, A. J.; Beard, M. C. *Nano Lett.* **2011**, *11*, 1002–1008.
- (2) Luther, J. M.; Gao, J.; Lloyd, M. T.; Semonin, O. E.; Beard, M. C.; Nozik, A. J. *Adv. Mater.* **2010**, *22*, 3704–3707.
- (3) Chen, L.-M.; Xu, Z.; Hong, Z.; Yang, Y. *J. Mat. Chem.* **2010**, *20*, 2575–2598.
- (4) Choi, J. J.; Lim, Y.; Santiago-Berrios, M. B.; Oh, M.; Hyun, B.; Sun, L.; Bartnik, A. C.; Goedhart, A.; Malliaras, G. G.; Abruña, H. D.; Wise, F. W.; Hanrath, T. *Nano Lett.* **2009**, *9*, 3749–3755.
- (5) Leschkies, K. S.; Beatty, T. J.; Kang, M. S.; Norris, D. J.; Aydil, E. S. *ACS Nano* **2009**, *3*, 3638–3648.
- (6) Tokito, S.; Noda, K.; Taga, Y. *J. Phys. D* **1996**, *29*, 2750–2753.
- (7) Li, J. H.; Huang, J.; Yang, Y. *Appl. Phys. Lett.* **2007**, *90*, 173505.
- (8) Matsushita, T.; Kinoshita, Y.; Murata, H. *Appl. Phys. Lett.* **2007**, *9*, 1253504.
- (9) You, H.; Da, Y.; Zhang, Z.; Ma, D. *Org. Electron.* **2008**, *9*, 985–993.
- (10) Kim, D. Y.; Subbiah, J.; Sarasqueta, G.; So, F.; Ding, H.; Irfan, Gao, Y. *Appl. Phys. Lett.* **2009**, *95*, 093304.
- (11) Subbiah, J.; Kim, D. Y.; Hartel, M.; So, F. *Appl. Phys. Lett.* **2010**, *96*, 063303.
- (12) Tao, C.; Ruan, S.; Zhang, X.; Xie, G.; Shen, L.; Kong, X.; Dong, W.; Liu, C.; Chen, W. *Appl. Phys. Lett.* **2008**, *93*, 193307.
- (13) Tao, C.; Ruan, S.; Zhang, X.; Xie, G.; Kong, X.; Shen, L.; Meng, F.; Liu, C.; Zhang, X.; Dong, W.; Chen, W. *Appl. Phys. Lett.* **2009**, *94*, 043311.
- (14) Li, G.; Chu, C. W.; Shrotriya, V.; Huang, J.; Yang, Y. *Appl. Phys. Lett.* **2006**, *88*, 253503.
- (15) Shrotriya, V.; Li, G.; Yao, Y.; Chu, C. W.; Yang, Y. *Appl. Phys. Lett.* **2008**, *88*, 073508.

- (16) Chen, L. M.; Xu, Z.; Hong, Z.; Yang, Y. *J. Mater. Chem.* **2010**, *20*, 2575–2598.
- (17) Semonin, O. E.; Luther, J. M.; Chen, H. Y.; Choi, S.; Gao, J.; Nozik, A. J.; Beard, M. C. To be submitted.
- (18) Cheung, C. H.; Song, W. J.; So, S. K. *Org. Electron.* **2010**, *11*, 89–94.
- (19) Kanai, K.; Koizumi, K.; Ouchi, S.; Tsukamoto, Y.; Sakanoue, K.; Ouchi, Y.; Seki, K. *Org. Electron.* **2010**, *11*, 188–194.
- (20) Woodhouse, M.; Perkins, C. L.; Rawls, M. T.; Cormier, R. A.; Liang, Z.; Nards, A. M.; Gregg, B. A. *J. Phys. Chem. C* **2010**, *114*, 6784–6790.
- (21) Kröger, M.; Hamwi, S.; Meyer, J.; Riedl, T.; Kowalsky, W.; Kahn, A. *Appl. Phys. Lett.* **2009**, *95*, 123301.
- (22) Meyer, J.; Shu, A.; Kröger, M.; Kahn, A. *Appl. Phys. Lett.* **2010**, *96*, 133308.
- (23) Irfan, H.; Ding, Y.; Gao, D. Y.; Kim, J.; Subbiah, F. *Appl. Phys. Lett.* **2010**, *96*, 073304.
- (24) Irfan, H.; Ding, Y.; Gao, C.; Small, D. Y.; Kim, J.; Subbiah, F. *Appl. Phys. Lett.* **2010**, *96*, 243307.
- (25) Hancox, I.; Sullivan, P.; Chauhan, K. V.; Beaumont, N.; Rochford, L. A.; Hatton, R. A.; Joes, T. S. *Org. Electron* **2010**, *11*, 2019–2025.